Theoretical study of silver nanoparticle suspension in electroosmosis flow through a nonuniform divergent channel with compliant walls

A therapeutic application

Irfan, Muhammad; Siddique, Imran; Nazeer, Mubbashar; Ali, Waqas

DOI
10.1016/j.aej.2023.11.083

Publication date
2023

Document Version
Final published version

Published in
Alexandria Engineering Journal

Alexandria Engineering Journal 86 (2024) 443–457

Contents lists available at ScienceDirect

Alexandria Engineering Journal

journal homepage: www.elsevier.com/locate/aej

Theoretical study of silver nanoparticle suspension in electroosmosis flow through a nonuniform divergent channel with compliant walls: A therapeutic application

Muhammad Irfan [a], Imran Siddique [b], Mubbashar Nazeer [c], Waqas Ali [d,*]

[a] Department of Mathematics (SSC), University of Management and Technology C-II, Johar Town, Lahore, Pakistan
[b] Department of Mathematics, University of Sargodha, 40162, Pakistan
[c] Department of Mathematics, Institute of Arts and Sciences, Government College University Faisalabad Chiniot Campus, 35400, Chiniot, Pakistan
[d] Department of Hydraulic Engineering, Delft University of Technology, Netherlands

ARTICLE INFO

Keywords:
Compliant walls
Nanofluid
Nonuniform channel
Silver nanoparticles
Ellis model

ABSTRACT

This study explores the effect of silver nanoparticles on heat transfer and flow behavior within the context of the Ellis fluid model. It specifically considers electroosmotic forces in a nonuniform divergent channel with compliant walls. The analysis involves studying thermal transport in silver-blood nanofluid flow, using MATHEMATICA 13.2 software to obtain exact solutions for velocity and temperature distribution. Findings reveal that certain parameters, such as wall damping and wall elastic properties, increase skin friction, while compliant wall parameters generally reduce flow velocity. Additionally, wall rigidity and tension parameters lead to larger trapped boluses. Notably, a 1% concentration of nanoparticles enhances heat transfer by up to 13.75%, offering control over heat transfer rates. This research introduces a novel perspective by examining compliant wall impacts on heat transfer analysis in the context of electroosmotic flow within the Ellis fluid model, incorporating silver nanoparticles with potential therapeutic applications due to their antibacterial properties.

1. Introduction

A sufficient amount of research is organized by scientists and researchers to explore the applications of nanofluids in the fields of engineering and technology. The low thermal conductivity of nanofluids follows a certain issue during the limited investigation of thermal transport. This subject can be solved by adding suitable volumetric concentrations of nanoparticles of higher thermal conductivity in the domain of base fluid. These types of particles are made of matter, and the size of their diameter ranges from 1nm to100nm. The nanoparticles of noble metals (Au and Ag) have peculiar nature and flexibility, which play a vital role in many industrial and engineering applications. The copper nanoparticles and their alloys play an important role in nanotechnology, like modelling design of operating devices, microbial fuel cells, food processing, biomedical applications, cancer treatment, microelectronic devices, energy storage, etc. [1–4]. Jiang et al. [5] studied the catalytic properties of silver nanoparticles and used these particles as catalysts. Boumegnane et al. [6] investigated silver nanoparticles for wearable electronic applications. Kowalczyk et al. [7] presented medical and microbiological applications of silver nanoparticles. Bruna et al. [8] used silver nanoparticles for antibacterial applications.

The movement of a biofluid (or a physiological fluid) in a channel or tube due to sinusoidal waves is known as peristaltic flow. The peristaltic flow has a wide range of applications in the field of biomedical engineering. Many researchers and scholars mathematically investigated the peristaltic motion of nanofluid flow to study the heat transfer rate. Akbar et al. [9] investigated unsteady peristaltic nanofluid flow through irregular channels with carbon nanotubes for cancer treatment. Mahendra et al. [10] studied the Eyring Powell peristaltic fluid flow in asymmetrical channels for gyrotactic microbes, which are useful for cardiac surgery. Mishra et al. [11] analyzed the peristaltic transport of two-dimensional fluid flow in the peripheral region of the gastrointestinal tract. Tripathi and Beg [12] studied peristaltic nanofluid flow through the two-dimensional channel for drug delivery application. Mekheimer and Elmaboud [13] observed the peristaltic motion of Newtonian nanofluid in a vertical annulus for endoscopic application. The peristaltic motion of Bingham plastic fluid through a vertical

* Corresponding author.
E-mail address: w.ali@tudelft.nl (W. Ali).

https://doi.org/10.1016/j.aej.2023.11.083
Received 20 July 2023; Received in revised form 22 November 2023; Accepted 29 November 2023
Available online 7 December 2023

Nomenclature

$\mathbf{V}$	The velocity vector (m/s)
ρ_{nf}	The density of nanofluid (kg/m^3)
T	The temperature (K)
k_{nf}	The thermal conductivity of nanofluid (W/mK)
$\mathbf{D}$	The material derivative
$\mathbf{A_1}$	The Rivilin-Ericksen tensor
μ	The dynamic viscosity
U	The velocity component in $x-$ axis direction (m/s)
t	The time (s)
E_Y	The electric field component in the $Y-$ axis direction (V/m)
ρ_e	The density of symmetrical electrolytes
n_{e-}	The number of densities for anion
Đ	The Boltzmann constant
δ	The wave number
E_2	The wall tension parameter
E_4	The damping nature of the wall
Re	Reynolds number
Br	Brinkmann number
η_1	The mass per unit area
η_2	The viscosity coefficient for damping wall
k_s	The thermal conductivity of nanoparticles (W/mK)
ϕ	The volumetric concentration of nanoparticles
ρ_s	The density of nanoparticles (kg/m^3)
μ_{nf}	The viscosity of nanoparticles $\left(\text{kg}\quad m^{-1}s^{-1}\right)$
k	Electroosmotic parameter
Zh	The heat transfer rate
ψ	The stream function
λ	The wavelength (m)
T_1	The temperature of the upper wall (K)
$\mathbf{S}$	The extra stress tensor $\left(\frac{N}{m^2}\right)$
P	The pressure $\left(\frac{N}{m^2}\right)$
$\mathbf{E}$	The electric field
$(\rho c_p)_{nf}$	Heat capacity of nanofluid
ρ_e	The electric charge density
α	The material parameter
τ_0	The material constant
V	The velocity component in $Y-$ axis direction (m/s)
E_x	The electric field component in the $x-$ axis direction (V/m)
ϵ	The electric permittivity
n_{e+}	The number of densities for cation
K_B	The diffusion coefficient $\left(\frac{m^2}{s}\right)$
T_n	The Absolute temperature (K)
E_1	The wall rigidity
E_3	The mass characterization parameter
E_5	An elastance of wall
Ec	Eckert number
τ	The elastic tension parameter
η_3	The flexural rigidity of the walls of the channel
η	The stiffness
k_f	The thermal conductivity of the base fluid (W/mK)
ρ_f	The density of the base fluid (kg/m^3)
μ_f	The viscosity of the base fluid $\left(\text{kg}\quad m^{-1}s^{-1}\right)$
C_{sf}	The skin friction coefficient
β	The material parameter
θ	The dimensionless temperature (K)
a	The wave amplitude (m)
T_0	The temperature of the lower wall (K)
u	The dimensionless velocity component in the axial direction (m/s)

asymmetric channel was studied by Muthuraj et al. [14]. The heat transfer rate of peristaltic motion under electrokinetic effects of Jeffery fluid flow is investigated through the microchannel and nonuniform channels by Manjunatha et al. [15] and Rajashekhar et al. [16], respectively.

When two conducting phases (positive and negative) are attached, EDL (electrical double layer) is formed [17]. Thus, due to the variation of electric potential near the surface, the colloidal solution has significant behaviour during nanofluid flow. The flow of fluid contacting with a charged solid surface in the presence of an electric field is known as electroosmotic flow [18]. Electroosmotic flow has applications in the field of micro liquid chromatography systems [19,20], microflow injection analysis [21,22], microreactors [23], micro energy systems [24], microelectronic cooling systems [25], and micro physiological system [26]. The circulation of blood nanofluid under the effects of EDL through endoscopy and diverging fatty arteries is investigated for biomedical processes and therapeutic implications [27,28]. Islam et al. [29] observed the electroosmotic effects on blood circulatory regimen flow with swimming microbes and activation energy. Irfan et al. [30] studied the electroosmotic peristaltic motion of Casson nanofluid through a symmetric complex wavy channel. Their study was based on a blood-gold nanofluid with four different shapes of nanoparticles and concluded that the spherical shape is more effective for detecting and treating cancer. Nazeer et al. [31] investigated the Casson nanofluid under the effects of thermal radiation and electroosmosis to calculate the entropy generation. Their study is useful for the application of skin diseases. Maraj et al. [32] studied the peristaltic motion of methanol-based nanofluid through the nonuniform channel under the electroosmotic effects. They assumed the copper nanoparticles of different shapes to improve the design of the drug and delivery.

The properties of elastic walls strongly affect the flow behaviour through nonuniform channels due to the dependence of mean pressure, flow rate, and axial velocity on elastic wall properties. During the peristaltic motion of blood flow in veins and arteries, air flow in the lungs, and urine flow in the urethra, the assumption of wall properties is essential. Srinivas and Kothandapani [33] investigated the heat transfer rate through porous space with compliant walls. Ali et al. [34] analyzed the urine transport from the kidney to the bladder by considering the Maxwell fluid flow model through a channel having complaint walls. Bhattacharyya et al. [35] compared the results of the peristaltic motion of Eyring-Powell fluid under the effects of joule heating through uniform and nonuniform channels with properties of flexible walls. Eldesoky et al. [36] investigated the complaint wall properties, heat transfer, and slip conditions for peristaltic transport through tubes. Pandey and Chaube [37] presented the properties of the compliant wall for the peristaltic motion of a Couple stress fluid through the channel. To study the heat transfer rate, Vaidya et al. [38] investigated Rabinowitsch fluid over the inclined channel with compliant walls. Muthuraj et al. [39] studied the wall properties of the dusty fluid to investigate the heat transfer rate in an asymmetrical vertical channel.

Viscosity is the essential property of the fluid, which divides the fluid into two major types, i.e., Newtonian and non-Newtonian fluids. The contribution of non-Newtonian fluids in engineering, technology, and medicine plays a huge role. The study of non-Newtonian fluids is not an easy task because of their complex nature. The scientists and researchers tried the different non-Newtonian fluid models to study the complex

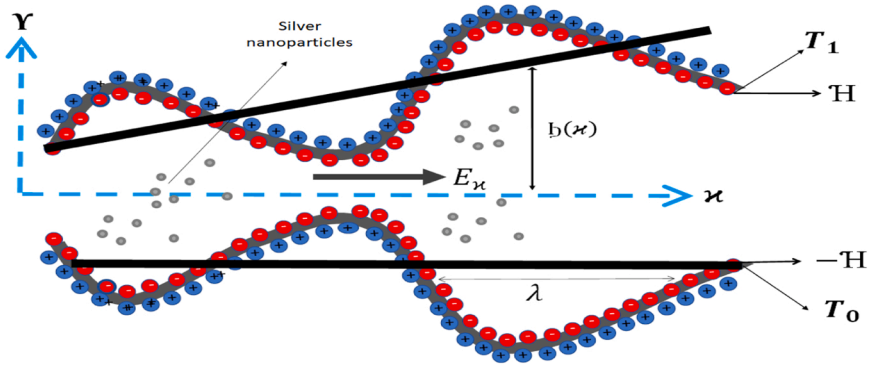

Fig. 1. Geometry of current flow problem.

behaviour of various non-Newtonian fluids like Carreau fluid [40], Buongiorno two-phase nanofluid model [41], generalized Burger's fluid [42], Sisko fluid [43], third-grade fluid [44], fourth-grade [45], Couple stress fluid [46], Jeffrey fluid [47,48], Eyring Powell [49], Hamilton and Cross model [50], Herschel–Bulkley Model [51] etc.

Another important fluid model is the Ellis fluid model (a generalized Newtonian fluid model), used in various medical science and technology applications. This fluid model shows Newtonian and non-Newtonian behaviour at small and large shear stress values. The distinct nature of the Ellis fluid model exactly suits blood circulation in the human body. Many researchers and scholars are working on Ellis's fluid model in different geometries. This current analysis is performed to investigate the impact of silver nanoparticles on the heat transfer rate and flow field of the Ellis fluid model with electroosmotic forces through a nonuniform divergent channel with compliant walls. This investigation is useful for therapeutic applications like cancer therapy, tumour therapy, hyperthermia, and biomedical imaging. The present study emphasizes the following research equations.

- Why Ellis fluid model is helpful for blood circulation in the human body?
- What are the effects of compliant walls on silver-blood nanofluid through nonuniform channels?
- How are silver nanoparticles important because of their antibacterial properties?
- How momentum transport, thermal transport, heat transfer rate, and skin friction vary under the effects of various parameters.

2. Model of current flow

2.1. The geometry of flow problem

The current study investigates the electroosmotic two-dimensional flow of silver nanoparticles through nonuniform channels with compliant walls. The continuous waveform speed due to sinusoidal propagation at compliant walls is c. Let $\Upsilon = \pm\mathcal{H}(\varkappa, t)$ be the upper and lower walls of the nonuniform channel. The temperature assumed for the lower and upper walls is T_0 and T_1 respectively. Blood circulation occurs because of the electric field **E** in the axial direction. The cartesian coordinate system assumed in such a way that the centre line occurred in the $\varkappa$-axis in the direction of wave propagation and the Υ-axis taken as transverse to it. The geometry of wall deformation is defined [52] below and shown in Fig. 1.

$$\mathcal{H}(\varkappa, t) = \mathfrak{b}(\varkappa) + a Sin\frac{2\pi}{\lambda}(\varkappa - ct) \tag{1}$$

Where $\mathfrak{b}(\varkappa) = \mathfrak{b}_0 + \varsigma\varkappa$ defines the width of the half channel, a and λ denote the wave amplitude and wavelength respectively. The appropriate boundary conditions for current fluid flow are defined as

$$\frac{\partial U}{\partial \Upsilon} = 0 \quad at \quad \Upsilon = 0, U = 0, T = T_0 \quad at \quad \Upsilon = -\mathcal{H}, U = 0, T = T_1 \quad at \quad \Upsilon = \mathcal{H} \tag{2}$$

2.2. Formulation of Problem

In the present investigation, the electroosmotic Ellis nanofluid flow model is selected for the impacts of various physical parameters on silver-blood nanofluids. The antibacterial properties of silver nanoparticles are useful for therapeutic applications. The blood circulation in the human body is precisely suited to this model. Because the Ellis nanofluid flow model behaves like Newtonian fluid flow at small shear stress and Newtonian at large shear stress. The electroosmotic effects and compliant wall effects are also added in this model during the thermal transport of silver nanoparticles in human blood circulation, which is why the nonuniform channel is suggested for this flow. The momentum and energy equations of current flow are defined as [53–55].

$$\nabla.\mathbf{V} = 0, \tag{3}$$

$$\rho_{nf} D\mathbf{V} = -\nabla P + \nabla.\mathbf{S} + \rho_e \mathbf{E} \quad , \tag{4}$$

$$(\rho c_p)_{nf} DT = -k_{nf}\nabla^2 T + Tra(\mathbf{S}.\nabla\mathbf{V}). \tag{5}$$

Where $\mathbf{V}, \mathbf{D}, \rho_{nf}, \mathbf{E}, \rho_e, k_{nf}, (\rho c_p)_{nf}, P, \mathbf{T}$, and $\mathbf{S}$ denote the velocity, material derivative, density of nanofluid, electric field, electric charge density, thermal conductivity of nanofluid, the heat capacity of nanofluid, hydrostatic pressure, temperature, and extra stress tensor respectively. The stress tensor of Ellis nanofluid is defined as [55].

$$\mathbf{S} = \frac{\mu}{\left(1 + \frac{\Pi_S}{\tau_0}\right)^{\alpha-1}}\mathbf{A_1}. \tag{6}$$

Where μ denotes the dynamic viscosity, τ_0 is material constants, α is known as a material parameter, Π_S denotes second-order invariant stress tensor and $\mathbf{A_1}$ is first Rivilin-Ericksen tensor. Usually, τ_0 express the shear stress related to half dynamic viscosity. As $\frac{1}{\tau_0^2} \to 0$ and $\alpha = 1$, the model (6) transformed to Newtonian model. For two-dimensional flow velocity, **V** can be defined as $\mathbf{V} = [U(\varkappa, \Upsilon, t), V(\varkappa, \Upsilon, t), 0]$. Where $U(\varkappa, \Upsilon, t)$ and $V(\varkappa, \Upsilon, t)$ are velocity components in $\varkappa$ and Υ direction, respectively. Using Eq. (6) and Eqs. (3–5) following scalar equations are obtained.

$$\frac{\partial U}{\partial \varkappa} + \frac{V}{\partial \Upsilon} = 0, \tag{7}$$

$$\rho_{nf}\left(\frac{\partial U}{\partial t} + U\frac{\partial U}{\partial \varkappa} + V\frac{\partial U}{\partial \Upsilon}\right) = -\frac{\partial P}{\partial \varkappa} + \frac{\partial}{\partial \varkappa}S_{\varkappa\varkappa} + \frac{\partial}{\partial \Upsilon}S_{\varkappa\Upsilon} + \rho_e E_\varkappa, \tag{8}$$

$$\rho_{nf}\left(\frac{\partial V}{\partial t}+U\frac{\partial V}{\partial x}+V\frac{\partial V}{\partial Y}\right)=-\frac{\partial P}{\partial Y}+\frac{\partial}{\partial x}S_{Yx}+\frac{\partial}{\partial Y}S_{YY}+\rho_e E_Y, \tag{9}$$

$$(\rho c_p)_{nf}\left(\frac{\partial T}{\partial t}+U\frac{\partial T}{\partial x}+V\frac{\partial T}{\partial Y}\right)=-k_{nf}\left(\frac{\partial^2 T}{\partial x^2}+\frac{\partial^2 T}{\partial Y^2}\right)+S_{xx}\frac{\partial U}{\partial x}+S_{YY}\frac{\partial V}{\partial Y}+\left(\frac{\partial V}{\partial x}+\frac{\partial U}{\partial Y}\right)S_{xY}. \tag{10}$$

Where S_{xx}, S_{xY} and S_{YY} are the components of the stress tensor, E_x and E_Y denote the components of the electric field. The electric charge density ρ_e defined by using the Boltzmann equation [52].

$$\nabla^2\varphi=-\frac{\rho_e}{\epsilon}. \tag{11}$$

Where φ denotes the electric potential and ϵ denotes the electric permittivity. The electric charge ρ_e density for symmetrical electrolytes can be defined as

$$\rho_e=ez(n_+-n_-). \tag{12}$$

Where the number of densities for cation and anion is denoted by n_+ and n_- respectively. The relation of electric potential with these numbers can be defined by using the Nernst-Planck (NP) equation as

$$\frac{\partial n_\pm}{\partial t}+U\frac{\partial n_\pm}{\partial x}+V\frac{\partial n_\pm}{\partial Y}=D\left(\frac{\partial^2 n_\pm}{\partial x^2}+\frac{\partial^2 n_\pm}{\partial Y^2}\right)\pm\frac{Dze}{K_B T_n}\left(\frac{\partial}{\partial x}\left(n_\pm\frac{\partial\varphi}{\partial x}\right)+\frac{\partial}{\partial Y}\left(n_\pm\frac{\partial\varphi}{\partial Y}\right)\right). \tag{13}$$

Where K_B is diffusion coefficient, D is Boltzmann constant and T_n is temperature. Further, the Einstein formula is used to compute the mobility of species and the ionic diffusion coefficient assumed equal for two species. Some important transformation and dimensionless physical parameters are defined to simplify the above equations.

$$\left.\begin{gathered}\bar{x}=\frac{x}{\lambda},\bar{y}=\frac{Y}{b_0},\bar{t}=\frac{ct}{\lambda},\bar{u}=\frac{U}{c},\bar{v}=\frac{V}{c\delta},\bar{P}=\frac{b_0^2P}{\mu_f\lambda c},\bar{h}=\frac{H}{b_0},\bar{S}=\frac{b_0}{c\mu_f}S,\\ \delta=\frac{b_0}{\lambda},\Theta=\frac{a}{b_0},\bar{\varphi}=\frac{ze}{K_BT}\varphi,\bar{n}_\pm=\frac{n_\pm}{n_0},\bar{\theta}=\frac{T-T_0}{T_1-T_0},\mathrm{Re}=\frac{\rho cb_0}{\mu_f},U_{HS}=-\frac{\xi\epsilon E_x}{\mu_f c}\\ \mathrm{Pr}=\frac{\mu_f}{c_fk_f},Ec=\frac{c^2}{c_f(T_1-T_0)},Br=PrE,E_1=-\beta\frac{b_0^3}{\lambda^3c\mu_f},E_2=\eta_1\frac{cb_0^3}{\lambda^3\mu_f}\\ E_3=\eta_2\frac{b_0^3}{\lambda^2\mu_f},E_4=\eta_3\frac{b_0^3}{\lambda^5c\mu_f},E_5=\eta\frac{b_0^3}{\lambda c\mu_f}\end{gathered}\right\}. \tag{14}$$

Where E_1, E_2, E_3, E_4 and E_5 represent wall rigidity, wall tension parameter, mass characterization parameter, damping nature of the wall, and elastance of wall respectively, δ is wave number, Re is Reynolds number, Ec is Eckert number, Br is Brinkmann number. By using longer wavelength and lower Reynolds number i.e., $\mathrm{Re}, \delta''1$. Eq. (10) can be transformed as

$$\frac{\partial^2\bar{\varphi}}{\partial\bar{y}^2}=-\frac{k^2(\bar{n}_+-\bar{n}_-)}{2}. \tag{15}$$

Where $k=b_0ze\sqrt{\frac{2n_0}{cK_BT_n}}$ is known as Deby length. Eq. (12) can be transformed as

$$+\frac{\partial}{\partial\bar{y}}\left(\frac{\partial\bar{\varphi}}{\partial\bar{y}}\right)=0. \tag{16}$$

Eq. (15) can be solved subject to the boundary condition $\bar{n}_\pm=1$, at $\bar{n}_\pm=0$ and $\frac{\partial\bar{n}_\pm}{\partial\bar{y}}=0$, at $\frac{\partial\bar{\varphi}}{\partial\bar{y}}=0$, then $\bar{n}_\pm=e^{\bar{\varphi}}$. Now Eq. (16) reduces to $\frac{\partial\bar{\varphi}}{\partial\bar{y}}=k^2Sin(\bar{\varphi})$. By using low zeta potential approximation for subsequential results we can write

$$\frac{\partial\bar{\varphi}}{\partial\bar{y}}=k^2\bar{\varphi}. \tag{17}$$

The above equation can be solved by assuming $\frac{\partial\bar{\varphi}}{\partial\bar{y}}=0$ at $\bar{y}=0$ and $\bar{\varphi}=1$ at $\bar{y}=\bar{h}$ to obtain

$$\bar{\varphi}=\frac{\cosh ky}{\cosh kh}. \tag{18}$$

In the view of longer wavelength approximation and lower Reynolds number, Eq. (1) and Eqs. (7)-(10) reduce to

$$\bar{h}=1+\frac{\mathscr{B}\bar{x}\lambda}{b_0}+\Theta\sin 2\pi(\bar{x}-\bar{t}), \tag{19}$$

$$\frac{\partial\bar{u}}{\partial\bar{x}}+\frac{\partial\bar{v}}{\partial\bar{y}}=0, \tag{20}$$

$$\frac{\partial\bar{P}}{\partial\bar{x}}=\frac{\partial}{\partial\bar{y}}S_{\bar{x}\bar{y}}+k^2U_{HS}\bar{\varphi}, \tag{21}$$

$$\frac{\partial\bar{P}}{\partial\bar{y}}=0, \tag{22}$$

$$R\frac{\partial^2\bar{\theta}}{\partial\bar{y}^2}=-\mu_{nf}BrS_{\bar{x}\bar{y}}\frac{\partial\bar{u}}{\partial\bar{y}}. \tag{23}$$

Where R is given in the appendix. From Eq. (6) we have

$$S_{\bar{x}\bar{y}}=\frac{\frac{\partial\bar{u}}{\partial\bar{y}}}{1+\left(\beta S_{\bar{x}\bar{y}}\right)^{a-1}}, \tag{24}$$

$$S_{\bar{y}\bar{y}}=S_{\bar{x}\bar{x}}=0. \tag{25}$$

The non-dimensional boundary condition from Eq. (2) transformed as

$$\frac{\partial\bar{u}}{\partial\bar{y}}=0,\frac{\partial\bar{\theta}}{\partial\bar{y}}=0at\quad\bar{y}=0,\bar{u}=0at\quad\bar{y}=\bar{h},\bar{u}=0,\bar{\theta}=0at\quad\bar{y}=-\bar{h} \tag{26}$$

2.3. Expression for compliant walls

The compliant walls expression can be given as

$$L(\bar{h})=\bar{P}-\bar{P}_0. \tag{27}$$

Where $\bar{P}_0$ is assumed to be zero because it shows the pressure due to tension in muscle outside the surface. Where the movement of the stretched membrane because of viscous damming force is described by operator L and defined [56] as

$$L=\beta\frac{\partial^2}{\partial\bar{x}^2}+\eta_1\frac{\partial^2}{\partial\bar{t}^2}+\eta_2\frac{\partial}{\partial\bar{t}}+\eta_3\frac{\partial^4}{\partial\bar{x}^4}+\eta. \tag{28}$$

Where β is the elastic tension parameter for the wall, η_1 denote the mass per unit area, η_2 expresses the viscosity coefficient for damping wall, η_3 shows the flexural rigidity of the walls of the channel and η represents the stiffness.

Using Eq. (25) - (26) we have

$$\frac{\partial\bar{P}}{\partial\bar{x}}=E_1\frac{\partial^3\bar{h}}{\partial\bar{x}^3}+E_2\frac{\partial^3\bar{h}}{\partial\bar{x}\,\partial\bar{t}^2}+E_3\frac{\partial^2\bar{h}}{\partial\bar{x}\,\partial\bar{t}}+E_4\frac{\partial^5\bar{h}}{\partial\bar{x}^5}+E_5\frac{\partial\bar{h}}{\partial\bar{x}}=\frac{\partial}{\partial\bar{y}}S_{\bar{x}\bar{y}}+\bar{\varphi}. \tag{29}$$

2.4. Thermophysical properties of nanofluid

The appropriate relationship for the thermophysical properties of nanofluid is given as [57].

$$\mu_{nf} = \frac{\mu_f}{(1-\phi)^{2.5}}, \tag{30}$$

$$\frac{k_{nf}}{k_f} = \frac{k_s + (m-1)k_f - \phi(m-1)(k_f - k_s)}{k_s + (m-1)k_f - \phi(k_f - k_s)}, \tag{31}$$

$$\rho_{nf} = \rho_f(1-\phi) + \rho_s\phi, \tag{32}$$

$$(\rho c)_{nf} = (\rho c)_f(1-\phi) + (\rho c)_s\phi. \tag{33}$$

Where $k_s, k_f, \mu_{nf}, \mu_f, \rho_f, \rho_s$ and ϕ represents the thermal conductivity of nanoparticles, the thermal conductivity of the base fluid, the viscosity of nanoparticles, the viscosity of the base fluid, the density of the base fluid, the density of nanoparticles, and the volumetric concentration of nanoparticles. Thermophysical properties for base fluid blood and silver nanoparticles [58–60] are shown in Table 1.

2.5. Exact solutions

The bar is removed for simplicity during the process of obtaining the exact solutions. To find the closed form of the velocity solution the value of S_{xy} from Eq. (21) with the value of $\mathfrak{a}$ from Eq. (18) put in Eq. (24) we have

$$\frac{\partial u}{\partial x} = \frac{\left(\frac{\partial P}{\partial x}\right)y - k\,\mathrm{Sech}[hk]\,\mathrm{Sinh}[ky]\,U_{\mathrm{HS}}}{\mu_{nf}} + \beta^{-1+\alpha}\left(\frac{\left(\frac{\partial P}{\partial x}\right)y - k\,\mathrm{Sech}[hk]\,\mathrm{Sinh}[ky]\,U_{\mathrm{HS}}}{\mu_{nf}}\right)^{\alpha}. \tag{34}$$

For arbitrary values of α it is difficult to solve the above equation. The above equation easily can be solved by considering the values of α from non-negative integers. We assumed a particular value of $\alpha = 3$ to solve the above equation with boundary conditions provided in Eq. (26). The mathematical software MATHEMATICA 13.2 with built-in command DSolve is used to obtain the exact solution for velocity as shown below

$$u = \frac{1}{24k^3{\mu_{nf}}^3}\left(\begin{array}{l} -6k^3\left(\frac{\partial P}{\partial x}\right)(h-y)(h+y)\left(2{\mu_{nf}}^2 + \left(-3A^2 + \left(\frac{\partial P}{\partial x}\right)^2(h^2+y^2)\right)\beta^2\right) \\ +A\left(\begin{array}{l} 6\left(4k^2{\mu_{nf}}^2 + 3\left(-A^2k^2 + 4\left(2+h^2k^2\right)\left(\frac{\partial P}{\partial x}\right)^2\right)\beta^2\right)\mathrm{Cosh}[hk] - \\ 6\left(4k^2{\mu_{nf}}^2 + 3\left(-A^2k^2 + 4\left(\frac{\partial P}{\partial x}\right)^2(2+k^2y^2)\right)\beta^2\right)\mathrm{Cosh}[ky] \\ -9Ak\left(\frac{\partial P}{\partial x}\right)\beta^2\mathrm{Cosh}[2ky] - 2A^2k^2\beta^2\mathrm{Cosh}[3ky] + k\beta^2(9A\left(\frac{\partial P}{\partial x}\right)\mathrm{Cosh}[2hk] \\ +k\beta^2\left(\begin{array}{c} 9A\left(\frac{\partial P}{\partial x}\right)\mathrm{Cosh}[2hk] + 2A^2k\mathrm{Cosh}[3hk] - 36h\left(\frac{\partial P}{\partial x}\right) \\ \left(4\left(\frac{\partial P}{\partial x}\right) + Ak\mathrm{Cosh}[hk]\right)\mathrm{Sinh}[hk] \end{array}\right) + \\ 144k\left(\frac{\partial P}{\partial x}\right)^2 y\beta^2\mathrm{Sinh}[ky] + 18Ak^2\left(\frac{\partial P}{\partial x}\right)y\beta^2\mathrm{Sinh}[2ky] \end{array}\right) \end{array}\right) \tag{35}$$

Where A is given in the appendix.

The solution of temperature can be obtained from Eq. (23) with the appropriate boundary conditions given in Eq. (26).

Table 1
Thermophysical properties of blood and silver at 20^0 C.

Properties	Silver (Ag)	Blood
Density (ρ)	10.500	1063
Thermal conductivity (k)	429	0.492
Heat capacity (c_p)	235	3594

Table 2
The values of physical parameters used in this analysis.

Name	Symbol	Range	References
Electroosmotic parameter	k	$(0, 20]$	[45,61]
Helmholtz -Smoluchowski velocity	U_{HS}	$(0, 10]$	[46,62]
The volumetric concentration of nanoparticle	ϕ	$[0, 0.4]$	[47,63]
Brinkmann number	Br	[0,5]	[48,64]
Elastic parameters	E_1, E_2, E_3, E_4, E_5	(0,1)	[49]

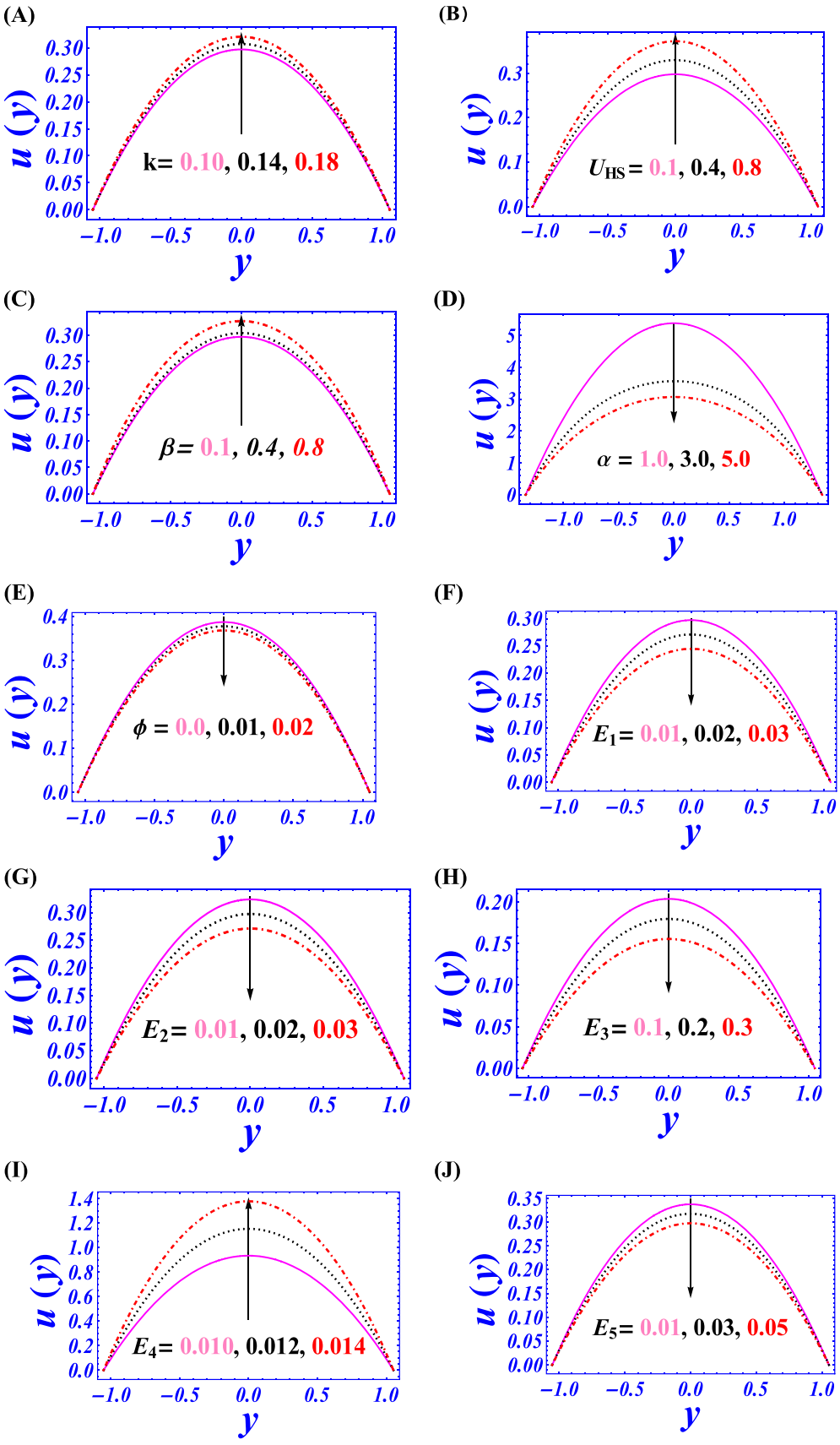

Fig. 2. Change in velocity for different parameters.

Table 3
Comparison of maximum velocity through uniform/nonuniform channel.

Parameters	Values	Velocity (Maximum) Uniform Channel	Velocity (Maximum) Nonuniform Channel
ϕ	0.00	1.1681	1.9916
	0.01	1.1378	1.9385
	0.02	1.1080	1.8861
k	0.1	1.1378	1.9385
	0.2	1.1766	2.0093
	0.3	1.2397	2.1219
U_{HS}	0.1	1.1378	1.9385
	0.2	1.1594	1,9628
	0.3	1.1641	1.9871
α	1.0	2.2212	3.7320
	3.0	1.1378	1.9385
	5.0	1.1115	1.8698
β	0.1	1.1378	1.9385
	0.2	1.2193	2.1560
	0.3	1.3552	2.2454

$$\theta = c_1 + {}_2y + \frac{1}{240}y^2\left(45a_{12} - 60a_9 - 10(a_{10} - 2a5)y^2 + 8a_6y^4\right) + \frac{1}{3456k^5}\left(-1728\text{Cosh}[ky]\left(\left(-3a_{11} + 4a_7\right)k^2 + 12a_8\left(4 + k^2y^2\right) + a_{10}k^2y\text{Sinh}[ky]\right) + k\left(216\left(2\left(-a_{12} + a_9\right)k^2 + a_{10}\left(3 + 2k^2y^2\right)\right)\text{Cosh}[2ky] + 62208a_8y\text{Sinh}[ky] + k\left(-64a_{11}\text{Cosh}[3ky] + 3k\left(9a_{12}\text{Cosh}[4ky] + 64y\left(-13a_{11} + 18\left(a_7 + a_8y^2\right) + a_{11}\text{Cosh}[2ky]\right)\text{Sinh}[ky]\right)\right)\right)\right). \tag{36}$$

Where $a_5 to a_{12}$, c_1 and c_1 are given in the appendix. The heat transfer rate for the lower plate is defined as

$$Zh = \left.\frac{\partial\theta}{\partial y}\right|_{y=-h}. \tag{37}$$

The skin friction for the lower plate is defined as

$$C_{sf} = \left.\frac{\partial u}{\partial y}\right|_{y=-h}\left(\frac{\partial h}{\partial x}\right).$$

The solution of streamlines is also part of the current study and is given below

$$\psi = -\frac{1}{360k^4\mathrm{U}_{nf}{}^3}\left(180h^2k^4\left(\frac{\partial P}{\partial x}\right)\mathrm{U}_{nf}{}^2y - 60k^4\left(\frac{\partial P}{\partial x}\right)\mathrm{U}_{nf}{}^2y^3 - 270A^2h^2k^4\left(\frac{\partial P}{\partial x}\right)y\beta^2 + 90h^4k^4\left(\frac{\partial P}{\partial x}\right)^3y\beta^2 + 90A^2k^4\left(\frac{\partial P}{\partial x}\right)y^3\beta^2 - 18k^4\left(\frac{\partial P}{\partial x}\right)^3y^5\beta^2 + 90Aky\left(-24\left(\frac{\partial P}{\partial x}\right)^2\beta^2 + k^2\left(-4\mathrm{U}_{nf}{}^2 + 3\left(A^2 - 4h^2\left(\frac{\partial P}{\partial x}\right)^2\right)\beta^2\right)\right)\text{Cosh}[hk] - 135A^2k^2\left(\frac{\partial P}{\partial x}\right)y\beta^2\text{Cosh}[2hk] - 30A^3k^3y\beta^2\text{Cosh}[3hk] - 4320Ak\left(\frac{\partial P}{\partial x}\right)^2y\beta^2\text{Cosh}[ky] - 135A^2k^2\left(\frac{\partial P}{\partial x}\right)y\beta^2\text{Cosh}[2ky] + 2160Ahk^2\left(\frac{\partial P}{\partial x}\right)^2y\beta^2\text{Sinh}[hk] + 270A^2hk^3\left(\frac{\partial P}{\partial x}\right)y\beta^2\text{Sinh}[2hk] + 360Ak^2\mathrm{U}_{nf}{}^2\text{Sinh}[ky] - 270A^3k^2\beta^2\text{Sinh}[ky] + 6480A\left(\frac{\partial P}{\partial x}\right)^2\beta^2\text{Sinh}[ky] + 1080Ak^2\left(\frac{\partial P}{\partial x}\right)^2y^2\beta^2\text{Sinh}[ky] + 135A^2k\left(\frac{\partial P}{\partial x}\right)\beta^2\text{Sinh}[2ky] + 10A^3k^2\beta^2\text{Sinh}[3ky]\Big). \tag{38}$$

3. Results and discussions

In previous sections, the literature is reviewed to develop a mathematical model of Ellis nanofluid flow with silver nanoparticles and blood as base fluid. The nonuniform channel with compliant walls is assumed to investigate the momentum transport, skin friction, thermal transport, heat transfer rate, and streamlines. The exact solution of governing equations is obtained using the mathematical software MATHEMATICA 13.2 using the built-in DSolve command.

This section is further divided into five subsections for a graphical representation of velocity, temperature, skin friction, heat transfer rate, and streamlines with trapping phenomenon under the effects of different parameters. Some important physical parameters and their range are defined in Table 2.

3.1. Transport of momentum

In this section, Fig. 2(A-J) illustrates the change of velocity corresponding to the electroosmotic parameter (k), Helmholtz -Smoluchowski velocity (U_{HS}), material parameters (α,β), the volumetric concentration of nanoparticles (ϕ), wall rigidity parameter (E_1), wall tension parameter (E_2), mass characterization parameter (E_3), wall damping parameter (E_4) and wall elastic parameter (E_5). In each graphical result of the main contributing parameter, the following numerical values of the remaining parameters are fixed. $\beta = 0.1, k = 1.0, U_{HS} = 1.0, \text{b}_0 = 3, t = 0, E_1 = 0.01, E_2 = 0.02, E_3 = 0.04, E_4 = 0.04, E_5 = 0.01$, $E_1 = 0.01x = 0.3$, $\lambda = 0.1$, $\phi = 0.01$. Fig. 2(A-B) shows the enlargement of the velocity profile for the electroosmotic parameter and Helmholtz-Smoluchowski velocity. Both parameters are related to EDL (electrical double layer), which becomes thin on the enhancement of U_{HS} and k. This factor accelerates the flow because the thin layer decreases the drag force. Fig. 2(C-D) illustrates the increasing behaviour of velocity with increasing values of material parameters β and the decreasing behaviour of velocity is noticed with increasing values of material parameter α. Fig. 2(E) shows that enhancing the volumetric concentration of nanoparticles diminishes the velocity profile because resistive force between the layers of base fluid increases, which impedes the flow accordingly. Fig. 2(F-H) shows the diminishing velocity behaviour for increasing the value of the wall rigidity, wall tension, and mass characterization parameters. Because wall rigidity, wall tension, and mass characterization parameters denote the shear resistance of the wall, systolic force by myocardial tissues, and mass of blood fluid in arteries. Fig. 2(I-J) explains the effects of the wall damping and elastic parameters on velocity. The wall damping parameter shows an enlargement of the velocity profile because the wall damping of arteries related to pulsatility pressure, anterograde wave generation, and systemic vascular resistance is reduced. However, the wall elastic parameter reduces the velocity because it relates to the elasticity of arteries. It is also noted that velocity is in parabolic shape in all cases.

In Table 3, the comparison of maximum velocity through uniform and nonuniform channels is provided in the region $-1 \le y \le 1$ for variation of each parameter by fixing the remaining parameters. It is noticed that velocity in nonuniform channels is prominent as compared to uniform channels. The velocity increases for material parameter β and EDL parameters, i.e., k and U_{HS} and decreases for material parameterα and volumetric concentration of nanoparticlesϕ, no matter whether the channel is uniform or nonuniform.

3.2. Analysis of skin friction

In this section, skin friction is plotted against longitudinal distance x. The results of each parameter are described by fixing the following parameters as $\beta = 0.1, k = 0.1, U_{HS} = 0.1, t = 0, E_1 = 0.01, E_2 = 0.01, E_3 = 0.04, E_4 = 0.001, E_5 = 0.001, E_1 = 0.01x = 0.3, \lambda = 0.1, \phi = 0.01$. In Fig. 3(A), the effects of electroosmotic parameter k are observed. Skin friction rises in the region $-0.75 < x < -0.25$ and diminishes in the

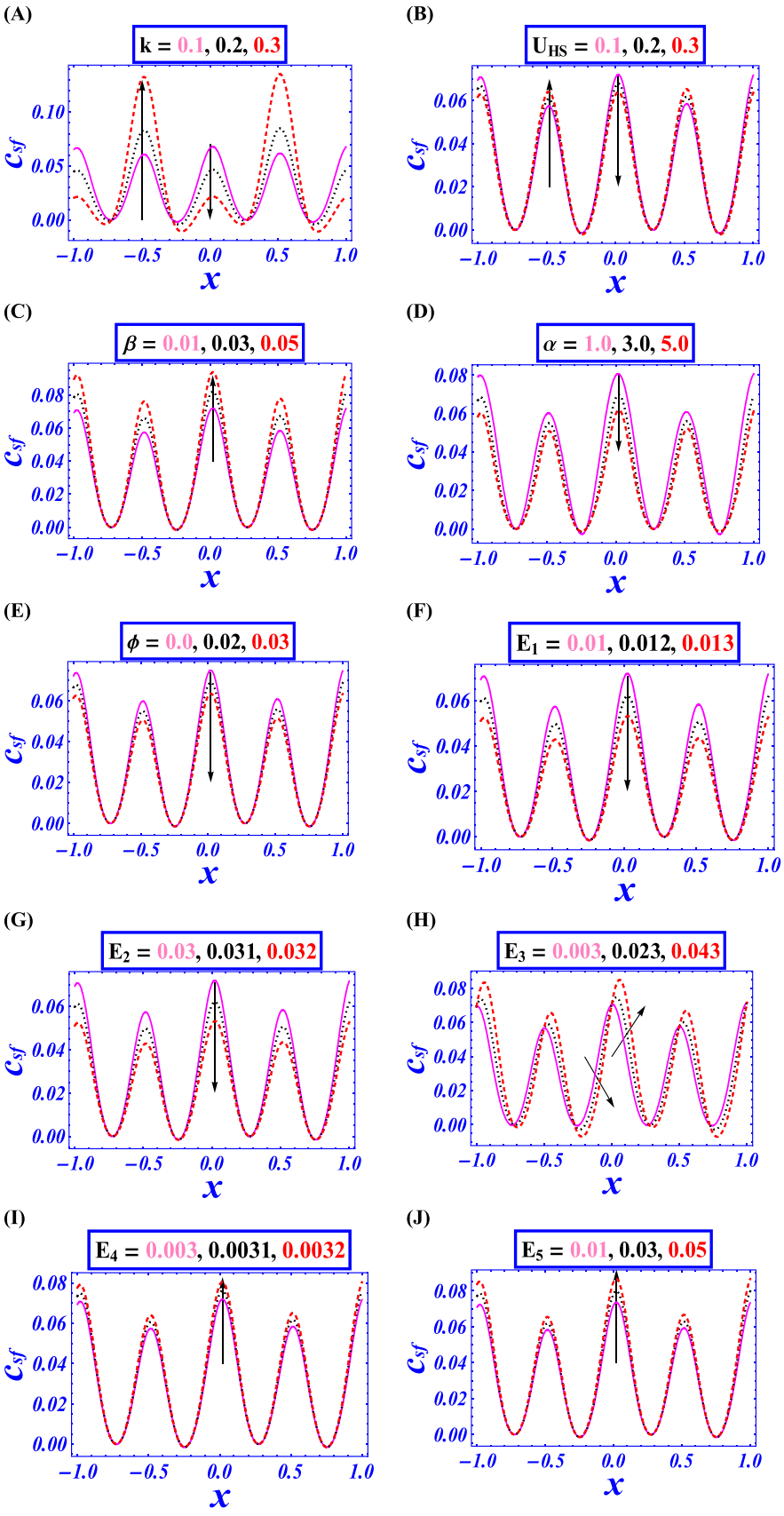

Fig. 3. The change in skin friction for various parameters.

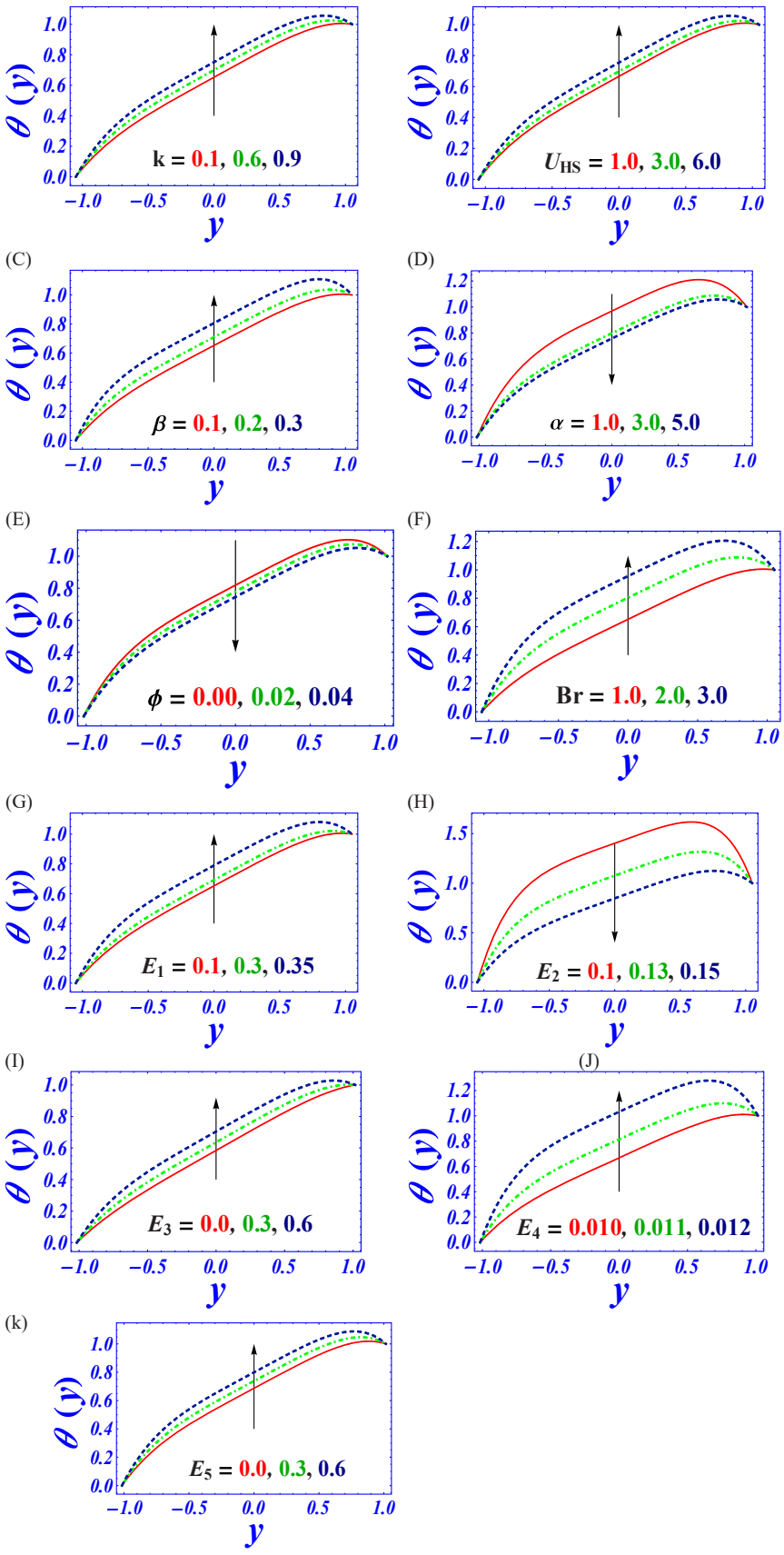

Fig. 4. Change in temperature for various parameters.

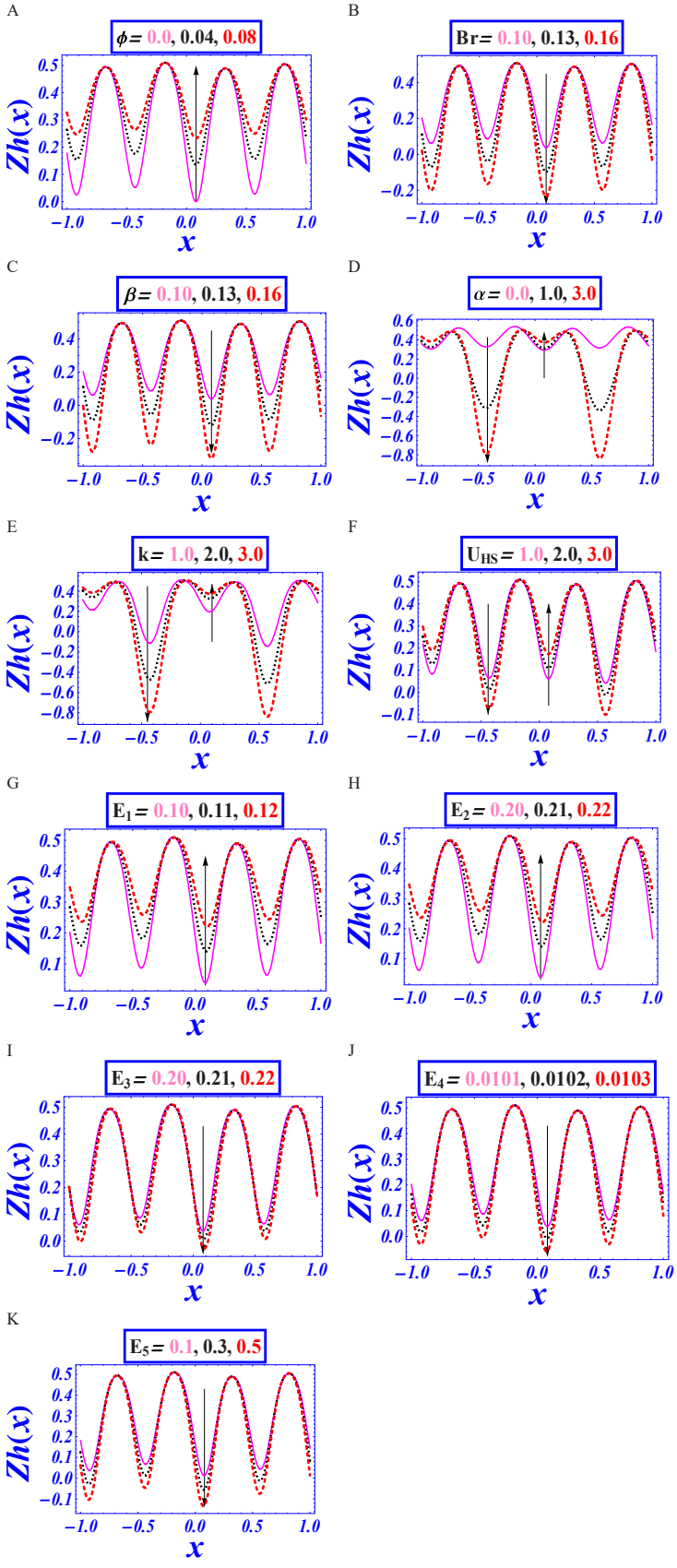

Fig. 5. The variation of heat transfer rate along longitudinal distance *x*.

Table 4
The percentage increase of heat transfer rate for variation of each parameter.

Parameters	Values	Heat transfer rate	Enhancement %	Increment/ Decrement
ϕ	0.0	0.1775	-	
	0.01	0.2019	13.75	Increasing
	0.02	0.2242	4.67	Increasing
k	0.1	0.2019	-	
	0.2	0.2072	0.53	Increasing
	0.3	0.2158	1.39	Increasing
U_{HS}	0.1	0.2019	-	
	0.2	0.2037	0.18	Increasing
	0.3	0.2055	0.36	Increasing
Br	0.1	0.2019	-	
	0.2	0.1715	3.04	Decreasing
	0.3	0.1413	6.06	Decreasing
β	0.10	0.2019	-	
	0.11	0.1739	2.80	Decreasing
	0.12	0.1435	5.84	Decreasing
α	1.0	0.1641	-	
	3.0	0.2019	3.78	Increasing
	5.0	0.8175	65.34	Increasing

region $-0.25 < x < 0.25$. In Fig. 3(B), skin friction under the effect of Helmholtz-Smoluchowski U_{HS} shows the same behaviour as shown in Fig. 3(A). In Fig. 3(C-D), interpret the results of skin friction under the effects of material parameters β and α. It is noticed that skin friction increases for material parameter β and decreases for material parameter α. In Fig. 3(E), the effects of nanoparticles' volumetric concentration on skin friction are plotted. It is observed that the volumetric concentration of nanoparticles reduces skin friction. Fig. 3(F-G) illustrates the graphical effects of the wall rigidity and tension parameters. These two parameters of compliant walls diminish skin friction. Fig. 3(H) demonstrates the effects of mass characterization parameters on skin friction. It is noticed that skin friction rises in the region $-0.25 < x < -0.25$ and diminishes in the region $-0.25 < x < 0$ for mass characterization parameters. Fig. 3(I-J) explains that the wall damping and elastic parameters boost skin friction.

3.3. Temperature variation

In this section, the thermal transport of Ellis nanofluid through the nonuniform channel is investigated under the variation of the main parameter with constant values of other parameters, as mentioned.$\beta = 0.1, \alpha = 3, k = 0.1, Br = 1, U_{HS} = 0.1, t = 0, E_1 = 0.1, E_2 = 0.2, E_3 = 0.3, E_4 = 0.4, E_5 = 0.5, x = 0.5, \phi = 0.01, Br = 1$. Fig. 4(A-B) shows the effects of electroosmotic parameter k and Helmholtz -Smoluchowski velocity U_{HS} on temperature. The increasing values of both parameters show an enhancement of the temperature profile. Fig. 4(C-D) exhibits the change in temperature profile under the effects of material parameters β and α. Enhancement in temperature profile is noticed with increasing values of material parameters β and material parameter α display diminishing behaviour of temperature profile. Fig. 4(E) shows the diminishing behaviour of the temperature profile due to enhancing the volumetric concentration of nanoparticles. Fig. 4(F) illustrates the graphical explanation of thermal transport due to variations in Brinkmann number. It is noticed that the Brinkmann number depicts the enhancement of the temperature profile. The reason behind this phenomenon is that the Brinkmann number boosts up the viscous dissipation, and the rise in viscous dissipation uplifts the temperature of the nanofluid. Fig. 4(G) shows the graphical illustration of the temperature profile under the effect of the wall rigidity parameter, and the temperature profile's enlargement is noticed. Fig. 4(G) demonstrates that the wall tension parameter declines the temperature profile. Fig. 4(I-K) shows the increasing behaviour of the temperature profile under the increasing value of the mass characterization, wall damping, and wall elastic parameters.

3.4. Investigation of heat transfer rate

This section presents a graphical sketch of the heat transfer rate for blood-silver Ellis nanofluid under the effects of EDL and compliant walls. It is plotted against the axial direction in the region $-1 \le x \le 1$. The variation of each parameter is illustrated in graphs by fixing the remaining parameters as $\beta = 0.1, k = 1.0, U_{HS} = 1.0, \mathfrak{h}_0 = 3, t = 0, E_1 = 0.01, E_2 = 0.02, E_3 = 0.04, E_4 = 0.04, E_5 = 0.01, E_1 = 0.01x = 0.3, \lambda = 0.1, \phi = 0.01, Br = 1$. Fig. 5(A) illustrates the heat transfer rate for the volumetric addition of nanoparticles. It is noticed that the volumetric concentration of nanoparticles increases the heat transfer rate. Fig. 5(B) shows the graphical effects of the heat transfer rate under the Brinkmann number. The diminishing behaviour of the heat transfer rate is observed because of the Brinkmann number. In Fig. 5(C), pictorial evidence of material parameter β on heat transfer rate is displayed. The material parameter β reduces the heat transfer rate. Fig. 5(D) demonstrates the effects of material parameter α on heat transfer rate. The effects of material parameter α are different from material parameter β. It is noticed that the heat transfer rate decreases in the region $-0.75 < x < -0.25$ and increases in the region $-0.25 < x < 0.25$ under the effects of material parameter α, and the same behaviour is noticed for the remaining region. It is also noticed that increasing behaviour is faster than decreasing behaviour. Fig. 5(E) presents the graphical effects of the electroosmotic parameter k on heat transfer rate. The graphical behaviour of the heat transfer rate for electroosmosis is the same as illustrated in Fig. 5(D). The effects of Helmholtz -Smoluchowski velocity U_{HS} on heat transfer rate expressed in Fig. 5(F). It is observed that the heat transfer rate gradually decreases in the region $-0.75 < x < -0.25$ and increases in the region $-0.25 < x < 0.25$. Fig. 5(G-H) illustrates the variation of heat transfer rate under the effects of the wall rigidity parameter E_1 and wall tension parameter E_2. These two parameters of compliant walls show heating effects due to the enhancement of the heat transfer rate. On the other hand, the mass characterization parameter E_3, wall damping parameter E_4 and wall elastic parameter E_5 show cooling effects, as shown in Fig. 5(J-K). Because these three parameters reduced the heat transfer rate, cooling effects are observed.

Table 4 shows the enhancement or decrement of the heat transfer rate percentage-wise. It is noticed that a 1% volumetric addition of nanoparticles ϕ increases the heat transfer rate up to 13.75%. Further, 2% volumetric concentration of nanoparticles causes to increase in the heat transfer rate slowly, i.e., 4.67%. Similarly, percentage enhancement is noticed for EDL parameters $(k, and \quad U_{HS})$ and material parameter α. Material β and Brinkmann parameter Br show a percentage decrement in heat transfer rate as presented in Table 4.

3.5. Visualization of streamlines

The trapping mechanism is one of the interesting and common phenomena in the peristaltic transport of bio-fluids. In the present study, the focus is on the creation of a circulating bolus bounded by closed streamlines. Creating a thrombus in blood and transporting food in the gas gastrointestinal tract are physical examples of the formation of the bolus. The variation of each parameter is sketched by fixing the remaining parameters as $\beta = 0.1, k = 1.0, U_{HS} = 1.0, \mathfrak{h}_0 = 3, t = 0, E_1 = 0.01, E_2 = 0.02, E_3 = 0.04, E_4 = 0.04, E_5 = 0.01, E_1 = 0.01x = 0.3, \lambda = 0.1, \phi = 0.01$. Fig. 6(A1-C1) and Fig. 6(A2-C2) show the effects of EDL parameters (electroosmotic parameter k and Helmholtz -Smoluchowski velocity U_{HS}) on closed streamlines to analyze the trapping phenomena. It is noticed that the enhancement of electroosmotic parameters and Helmholtz-Smoluchowski enhance the size of trapped boluses. Fig. 6 (A3-C3) and Fig. 6(A4-C4) show the effects of material parameters α and β on trapping bolus, respectively. The increasing value of material parameters α and β enhance the size of the trapped bolus and their numbers. Fig. 6(A5-C5) illustrates the effects of the volumetric concentration of nanoparticles on closed streamlines to observe the effects on trapped bolus. The size of the trapped bolus is reduced because of the

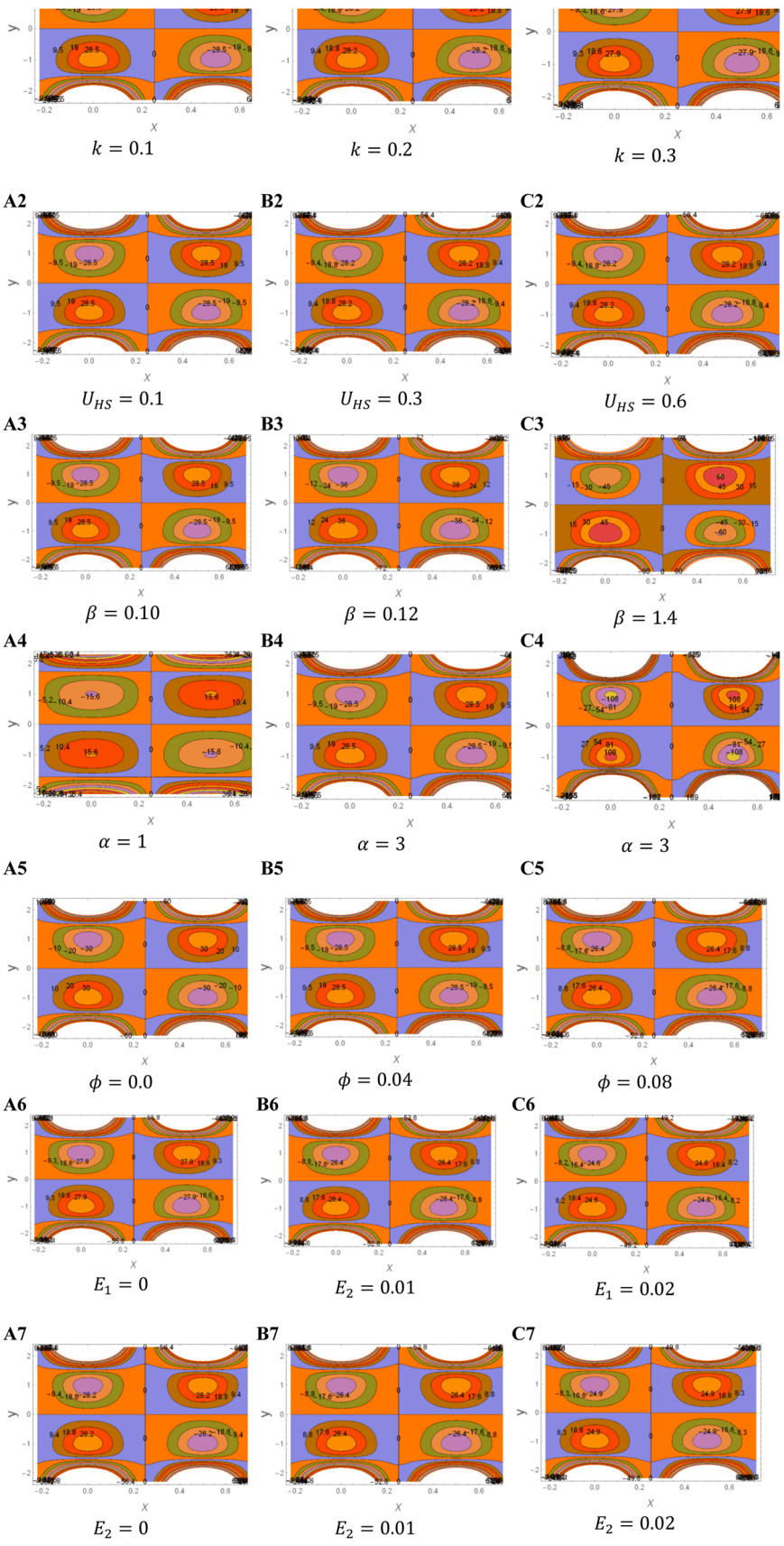

Fig. 6. Streamlines of the current flow.

volumetric concentration of nanoparticles. It depicts from Fig. 6(A6-C6) and Fig. 6(A7-C7) that increasing the value of the wall rigidity parameter E_1 and wall tension parameter E_2 decrease the size of the trapped bolus. Fig. 6(A8-C8) indicates the volume reduction of trapped bolus due to the mass characterization parameter E_3. This parameter also reduces the number of trapping bolus.

4. Conclusions

The rapid spread of infectious diseases poses a significant challenge in the contemporary era. Numerous scientists and researchers in engineering and technology are dedicated to mitigating the impact of such diseases. In the current study, we delve into the dynamics of blood circulation in the presence of silver nanoparticles within nonuniform channels with complementing walls. To investigate this phenomenon, we employ the Ellis nanofluid flow model, which exhibits a dual nature - behaving as a Newtonian fluid at low shear stress and a non-Newtonian fluid at higher stress levels. The governing partial differential equations (PDEs) are transformed into ordinary differential equations (ODEs) with appropriate boundary conditions. Subsequently, we obtain exact solutions for velocity and temperature using the mathematical software MATHEMATICA 13.2. We also calculate skin friction and heat transfer rates and visualize them graphically using the same software. Additionally, we create streamlined plots as a part of our investigation. The following key points were identified during this research.

- The velocity profile increases with increasing values of material parameter β and EDL parameters, i.e., k and U_{HS}. The velocity profile decreases for material parameters α and volumetric concentration of nanoparticles ϕ.
- The enhancement of temperature profile is noticed for parameter β, Brinkmann number Br and EDL parameters, i.e., k an U_{HS}. The decrement in temperature profile is noticed for material parameters α and volumetric concentration of nanoparticles ϕ.
- The skin friction increases for material parameter β and decreases for material parameter α and volumetric concentration of nanoparticles ϕ. The skin friction increases and reduces region-wise for EDL parameters.
- The enhancement in heat transfer rate was observed for volumetric concentration of nanoparticles ϕ and decreases for material parameter β, Brinkmann number Br.
- The percentage increment and decrement in the heat transfer rate are presented in the form of a Table.
- The comparison of velocity through uniform and nonuniform channels is illustrated in the form of a Table. It is noticed that the effects of various parameters are prominent in nonuniform channels.
- The trapping phenomenon is studied during the formulation of boluses. The size and number of boluses increase and decrease under the effects of various parameters.

- The compliant wall parameters decrease the velocity except for the wall-damping parameter E_4 and boost up the temperature profile except for the wall tension parameter E_2.
- Heat transfer rate rises for wall rigidity parameter E_1 and wall tension parameter E_2 but the other three compliant wall parameters decrease the heat transfer rate.
- The diminishing behaviour of skin friction is observed for E_1, E_2 and E_3.
- The trapping phenomenon is studied during the formulation of boluses. The size and number of boluses increase and decrease under the effects of various parameters.
- The size and number of trapped boluses are increased by wall rigidity and wall tension parameters.
- The size of the trapped boluses is reduced for E_3 and increases for E_4 and E_5
- This model is beneficial for Therapeutic Applications.

Scope of current work

This work is useful in biomedical, i.e., therapeutic applications.

Future direction

This study has the potential to expand to include hybrid nanofluid flow through porous media, analyzing various wave patterns (including square and triangular waves) under the effects of magnetic and thermal radiation parameters.

Declaration of Competing Interest

The authors declare that they have no known competing financial interests or personal relationships that could have appeared to influence the work reported in this paper.

Acknowledgment

The authors express gratitude to H. Khan and S. Saleem for their valuable contributions to this work.

Appendix

$$R=\frac{k_{nf}}{k_f}=\frac{k_s+(m-1)k_f-\phi(m-1)(k_f-k_s)}{k_s+(m-1)k_f-\phi(k_f-k_s)},A=\frac{kU_{\mathrm{HS}}}{\mathrm{Cosh}[kh]},$$

$$a_5=-\frac{\mathrm{Br}\left(\frac{\partial P}{\partial x}\right)^2}{R\mathrm{U}_{\mathrm{nf}}},a_6=-\frac{\mathrm{Br}\left(\frac{\partial P}{\partial x}\right)^4\beta^2}{R\mathrm{U}_{\mathrm{nf}}{}^3},a_7=\frac{2A\mathrm{Br}\frac{\partial P}{\partial x}}{R\mathrm{U}_{\mathrm{nf}}},a_8=\frac{4A\mathrm{Br}\left(\frac{\partial P}{\partial x}\right)^3\beta^2}{R\mathrm{U}_{\mathrm{nf}}{}^3},a_9=-\frac{A^2\mathrm{Br}}{R\mathrm{U}_{\mathrm{nf}}},a_{10}=-\frac{6A^2\mathrm{Br}\left(\frac{\partial P}{\partial x}\right)^2\beta^2}{R\mathrm{U}_{\mathrm{nf}}{}^3},a_{11}=\frac{4A^3\mathrm{Br}\frac{\partial P}{\partial x}\beta^2}{R\mathrm{U}_{\mathrm{nf}}{}^3},a_{12}=-\frac{A^4\mathrm{Br}\beta^2}{R\mathrm{U}_{\mathrm{nf}}{}^3},$$

$$\begin{aligned}c_1=&\frac{1}{17280k^5}(8640(48a_8+(-3a_{11}+4(a_7+3a_8h^2))k^2)\mathrm{Cosh}[hk]+k(72(120+15(-3a_{12}+4a_9)h^2+10(a_{10}-2a_5)h^4-8a_6h^6)k^4+5(-216(3a_{10}\\&+2(-a_{12}+a_9+a_{10}h^2)k^2)\mathrm{Cosh}[2hk]+64a_{11}k\mathrm{Cosh}[3hk]-27a_{12}k^2\mathrm{Cosh}[4hk]-192h(324a_8+(-13a_{11}+18(a_7+a_8h^2))k^2-9a_{10}k\mathrm{Cosh}[hk]\\&+a_{11}k^2\mathrm{Cosh}[2hk])\mathrm{Sinh}[hk]))),\end{aligned}$$

$$c_2 = \frac{1}{2h}$$

References

[1] H.F. Öztop, H. Coşanay, N. Biswas, F. Selimefendigil, Thermal energy storage via waste heat from finned heater by using different phase change materials in a closed space, J. Energy Storage 70 (2023), 108002.

[2] N. Biswas, D.K. Mandal, N.K. Manna, A.C. Benim, Magneto-hydrothermal triple-convection in a W-shaped porous cavity containing oxytactic bacteria, Sci. Rep. 12 (1) (2022).

[3] N. Biswas, D.K. Mandal, N.K. Manna, R.S.R. Gorla, A.J. Chamkha, Hybridized nanofluidic convection in umbrella-shaped porous thermal systems with identical heating and cooling surfaces, Int. J. Numer. Methods Heat. amp; Fluid Flow. 33 (9) (2023) 3164–3201.

[4] D.K. Mandal, N. Biswas, N.K. Manna, R.S. Gorla, A.J. Chamkha, Hybrid nanofluid magnetohydrodynamic mixed convection in a novel W-shaped porous system, Int. J. Numer. Methods Heat. amp; Fluid Flow. 33 (2) (2022) 510–544.

[5] Z.-J. Jiang, C.-Y. Liu, L.-W. Sun, Catalytic properties of silver nanoparticles supported on silica spheres, J. Phys. Chem. B 109 (5) (2005) 1730–1735.

[6] A. Boumegnane, A. Nadi, O. Cherkaoui, M. Tahiri, Inkjet printing of silver conductive ink on textiles for wearable electronic applications, Mater. Today.: Proc. 58 (2022) 1235–1241.

[7] P. Kowalczyk, M. Szymczak, M. Maciejewska, Ł. Laskowski, M. Laskowska, R. Ostaszewski, G. Skiba, I. Franiak-Pietryga, All that glitters is not silver—a new look at microbiological and medical applications of silver nanoparticles, Int. J. Mol. Sci. 22 (2) (2021) 854.

[8] T. Bruna, F. Maldonado-Bravo, P. Jara, N. Caro, Silver nanoparticles and their antibacterial applications, Int. J. Mol. Sci. 22 (13) (2021) 7202.

[9] N.S. Akbar, E.N. Maraj, N.F.M. Noor, M.B. Habib, Exact solutions of an unsteady thermal conductive pressure driven peristaltic transport with temperature-dependent nanofluid viscosity, Case Stud. Therm. Eng. 35 (2022), 102124.

[10] D.L. Mahendra, J.U. Viharika, V. Ramanjini, O.D. Makinde, U.B. Vishwanatha, Entropy analysis on the bioconvective peristaltic flow of gyrotactic microbes in Eyring-Powell nanofluid through an asymmetric channel, J. Indian Chem. Soc. 100 (3) (2023), 100935.

[11] M. Mishra, A.R. Rao, Peristaltic transport in a channel with a porous peripheral layer: Model of a flow in gastrointestinal tract, J. Biomech. 38 (4) (2005) 779–789.

[12] D. Tripathi, O.A. Bég, A study on peristaltic flow of nanofluids: application in drug delivery systems, Int. J. Heat. Mass Transf. 70 (2014) 61–70.

[13] Kh.S. Mekheimer, Y. Abd elmaboud, The influence of heat transfer and magnetic field on peristaltic transport of a newtonian fluid in a vertical annulus: Application of an endoscope, Phys. Lett. A 372 (10) (2008) 1657–1665.

[14] R. Muthuraj, S. Srinivas, D.L. Immaculate, Impacts of variable viscosity on hydromagnetic peristaltic flow of a Bingham fluid in a vertical channel, Lect. Notes Mech. Eng. (2022) 1–14.

[15] G. Manjunatha, C. Rajashekhar, H. Vaidya, K.V. Prasad, K. Vajravelu, Impact of heat and mass transfer on the peristaltic mechanism of Jeffery fluid in a nonuniform porous channel with variable viscosity and thermal conductivity, J. Therm. Anal. Calorim. 139 (2) (2019) 1213–1228, https://doi.org/10.1007/s10973-019-08527-8.

[16] C. Rajashekhar, F. Mebarek-Oudina, I.E. Sarris, H. Vaidya, K.V. Prasad, G. Manjunatha, H. Balachandra, Impact of electroosmosis and wall properties in modelling peristaltic mechanism of a Jeffrey liquid through a microchannel with variable fluid properties, Inventions 6 (4) (2021) 73, https://doi.org/10.3390/inventions6040073.

[17] R.J. Hunter, Zeta potential in Colloid Science: Principles and Applications, Academic Press, 1988.

[18] Li, S. Kevin, J. Hao, M. Liddell, Electrotransport across membranes in biological media: electrokinetic theories and applications in Drug Delivery, Transp. Biol. Media (2013) 417–454.

[19] C. Yan, D. Schaufelberger, F. Erni, Electrochromatography and micro high-performance liquid chromatography with 320 μm I.D. packed columns, J. Chromatogr. A 670 (1–2) (1994) 15–23, https://doi.org/10.1016/0021-9673(94)80276-9.

[20] M.A. Ramon, C. Fanali, S.D. Posta, G. D'Orazio, S. Fanali, Nano-liquid chromatography, Liq. Chromatogr. (2023) 177–226, https://doi.org/10.1016/b978-0-323-99968-7.00028-x.

[21] X. Wang, S. Wang, B. Gendhar, C. Cheng, C. Byun, G. LI, M. Zhao, S. Liu, C. Byun, M. Zhao, Electroosmotic pumps for microflow analysis, TrAC Trends Anal. Chem. 28 (1) (2009) 64–74, https://doi.org/10.1016/j.trac.2008.09.014.

[22] P.H. Petsul, G.M. Greenway, S.J. Haswell, The development of an on-chip micro-flow injection analysis of nitrate with a cadmium reductor, *Anal. Chim.* Acta 428 (2) (2001) 155–161, https://doi.org/10.1016/s0003-2670(00)01244-7.

[23] P. Karmakar, S. Das, Electro-blood circulation fusing gold and alumina nanoparticles in a diverging fatty artery, BioNanoScience 13 (2) (2023) 541–563, https://doi.org/10.1007/s12668-023-01098-x.

[24] P. Karmakar, A. Ali, S. Das, Circulation of blood loaded with trihybrid nanoparticles via electroosmotic pumping in an eccentric endoscopic Arterial Canal, Int. Commun. Heat. Mass Transf. 141 (2023), 106593, https://doi.org/10.1016/j.icheatmasstransfer.2022.106593.

[25] H.A. Alyousef, H. Yasmin, R. Shah, N.A. Shah, L.S. El-Sherif, S.A. El-Tantawy, Mathematical modeling and analysis of the steady electroosmotic flow of two immiscible fluids: A biomedical application, Coatings 13 (1) (2023) 115, https://doi.org/10.3390/coatings13010115.

[26] X. Wang, C. Cheng, S. Wang, S. Liu, Electroosmotic pumps and their applications in microfluidic systems, Microfluid. Nanofluidics 6 (2) (2009) 145–162, https://doi.org/10.1007/s10404-008-0399-9.

[27] Y. Han, Y.J. Lee, X. Zhang, Trapezoidal microchannel heat sink with pressure-driven and electroosmotic flows for microelectronic cooling, IEEE Trans. Compon., Packag. Manuf. Technol. 3 (11) (2013) 1851–1858, https://doi.org/10.1109/tcpmt.2013.2272478.

[28] J.C. Misra, G.C. Shit, S. Chandra, P.K. Kundu, Electroosmotic flow of a viscoelastic fluid in a channel: Applications to physiological fluid mechanics, Appl. Math. Comput. 217 (20) (2011) 7932–7939, https://doi.org/10.1016/j.amc.2011.02.075.

[29] S. Islam, B.M.J. Rana, Md.S. Parvez, Md.S. Hossain, M.M. Rahman, Electroosmotic flow in ternary (tio2-SIO2-al2o3) blood-based Sutterby nanomaterials with bio-active mixers, Int. J. Thermofluids 18 (2023), 100363.

[30] M. Irfan, M. Nazeer, F. Hussain, I. Siddique, Heat transfer analysis in the peristaltic flow of Casson nanofluid through asymmetric channel with velocity and thermal slips: Applications in a complex system, Int. J. Mod. Phys. B 36 (2022) 32.

[31] M. Nazeer, M. Irfan, F. Hussain, I. Siddique, M.I. Khan, K. Guedri, A.M. Galal, Analytical study of heat transfer rate of peristaltic flow in asymmetric channel with laser and magnetic effects: Remedy for autoimmune disease, Int. J. Mod. Phys. B 37 (2022) 03.

[32] E.N. Maraj, N.S. Akbar, I. Zehra, A.W. Butt, H. Ahmed Alghamdi, Electro-osmotically modulated Magneto hydrodynamic peristaltic flow of menthol based nanofluid in a uniform channel with shape factor, J. Magn. Magn. Mater. 576 (2023), 170774.

[33] S. Srinivas, M. Kothandapani, The influence of heat and mass transfer on MHD peristaltic flow through a porous space with compliant walls, Appl. Math. Comput. 213 (1) (2009) 197–208.

[34] N. Ali, T. Hayat, S. Asghar, Peristaltic flow of a Maxwell fluid in a channel with compliant walls, Chaos, Solitons Fractals 39 (1) (2009) 407–416.

[35] A. Bhattacharyya, R. Kumar, S. Bahadur, G.S. Seth, Sunil, Modeling and interpretation of peristaltic transport of eyring–powell fluid through uniform/nonuniform channel with joule heating and wall flexibility, Chin. J. Phys. 80 (2022) 167–182.

[36] I.M. Eldesoky, R.M. Abumandour, M.H. Kamel, E.T. Abdelwahab, The combined influences of heat transfer, compliant wall properties and slip conditions on the peristaltic flow through tube, SN Appl. Sci. 1 (8) (2019).

[37] S.K. Pandey, M.K. Chaube, Study of wall properties on peristaltic transport of a couple stress fluid, Meccanica 46 (6) (2010) 1319–1330.

[38] H. Vaidya, C. Rajashekhar, G. Manjunatha, K.V. Prasad, Peristaltic mechanism of a Rabinowitsch fluid in an inclined channel with complaint wall and variable liquid properties, J. Braz. Soc. Mech. Sci. Eng. 52 (2019) 41.

[39] R. Muthuraj, K. Nirmala, S. Srinivas, Influences of chemical reaction and wall properties on MHD peristaltic transport of a dusty fluid with heat and mass transfer, Alex. Eng. J. 55 (1) (2016) 597–611.

[40] M. Rooman, Z. Shah, E. Bonyah, M.A. Jan, W. Deebani, Mathematical modeling of Carreau fluid flow and heat transfer characteristics in the renal tubule, J. Math. 2022 (2022) 1–14. Article ID 2517933.

[41] P.M. Patil, M. Kulkarni, J.R. Tonannavar, A computational study of the triple-diffusive nonlinear convective nanoliquid flow over a wedge under convective boundary constraints, Int. Commun. Heat. Mass Transf. 128 (2021), 105561.

[42] Y. Abd Elmaboud, Electroosmotic flow of generalized burgers' fluid with Caputo–fabrizio derivatives through a vertical annulus with heat transfer, Alex. Eng. J. 59 (6) (2020) 4563–4575.

[43] J. Akram, N.S. Akbar, D. Tripathi, Numerical Study of the electroosmotic flow of al2o3–CH3OH Sisko nanofluid through a tapered microchannel in a porous environment, Appl. Nanosci. 10 (11) (2020) 4161–4176.

[44] S. Hina, S.M. Kayani, A. Fayyaz, Analysis of joule heating and hall effects on the electroosmotic flow of third-grade nanofluid regulated by peristaltic waves through a porous medium with double diffusion, Waves Random Complex Media (2023) 1–15.

[45] N. Fatima, M. Nazeer, M.M. Lashin, M.M. Ghafar, M.R. Gorji, M.K. Hameed, Developments of electroosmotic two-phase flows of fourth-grade fluid through convergent and divergent channels, Mathematics 11 (8) (2023) 1832.

[46] D. Tripathi, A. Yadav, O. Anwar Bég, Electroosmotic flow of couple stress fluids in a micro-channel propagated by peristalsis, Eur. Phys. J. 132 (4) (2017).

[47] M. Rafiq, M. Sajid, S.E. Alhazmi, M.I. Khan, E.R. El-Zahar, MHD electroosmotic peristaltic flow of Jeffrey nanofluid with slip conditions and chemical reaction, Alex. Eng. J. 61 (12) (2022) 9977–9992.

[48] C. Rajashekhar, H. Vaidya, F. Mebarek-Oudina, A. Wakif, M. Gudekote, K. Prasad, K. Vajravelu, S. Keriyapa, Electro-kinetically modulated peristaltic mechanism of Jeffrey liquid through a micro-channel with variable viscosity, Therm. Sci. 25 (Spec. issue 2) (2021) 271–277.

[49] Perumal, T., Rajaram, V., Arjunan, M. , 2023. Electroosmotic driven flow of Eyring Powell nanofluid in an asymmetric channel. Mathematical Methods in the Applied Sciences.
[50] P.M. Patil, S. Benawadi, Shape effects on the mixed convective hybrid nanoliquid flow over a rough slender cylinder with convective condition, Waves Random Complex Media (2022) 1–17.
[51] C. Rajashekhar, G. Manjunatha, K.V. Prasad, B.B. Divya, H. Vaidya, Peristaltic transport of two-layered blood flow using Herschel–Bulkley Model, Cogent Eng. 5 (1) (2018), 1495592.
[52] M.A. Abbas, M.M. Bhatti, M.M. Rashidi, Peristaltic blood flow of Ellis fluid through a nonuniform channel having compliant walls, J. Nanofluids 6 (2) (2017) 318–323.
[53] N. Ali, A. Abbasi, I. Ahmad, Channel flow of Ellis fluid due to peristalsis, AIP Adv. 5 (9) (2015), 097214.
[54] A. Abbasi, S.U. Khan, W. Farooq, F.M. Mughal, M. Ijaz Khan, B.C. Prasannakumara, M.T. El-Wakad, K. Guedri, A.M. Galal, Peristaltic flow of chemically reactive Ellis fluid through an asymmetric channel: Heat and mass transfer analysis, Ain Shams Eng. J. 14 (1) (2023), 101832.
[55] S. Saleem, F. Hussain, M. Irfan, I. Siddique, M. Nazeer, S.M. Eldin, Theoretical investigation of heat transfer analysis in Ellis nanofluid flow through the Divergent Channel, Case Stud. Therm. Eng. 48 (2023), 103140.
[56] M. Ali Abbas, Y.Q. Bai, M.M. Bhatti, M.M. Rashidi, Three dimensional peristaltic flow of hyperbolic tangent fluid in nonuniform channel having Flexible walls, Alex. Eng. J. 55 (1) (2016) 653–662.
[57] V. Sridhar, K. Ramesh, D. Tripathi, V. Vivekanand, Analysis of thermal radiation, joule heating, and viscous dissipation effects on blood-gold couple stress nanofluid flow driven by electroosmosis, Heat. Transf. 51 (5) (2022) 4080–4101.
[58] Y.-M. Chu, U. Khan, A. Shafiq, A. Zaib, Numerical simulations of time-dependent micro-rotation blood flow induced by a curved moving surface through conduction of gold particles with nonuniform heat sink/source, Arab. J. Sci. Eng. 46 (3) (2020) 2413–2427.
[59] A. Campo, N. Ben–Cheikh, A. Riahi, Water-based nanofluids for natural convection cooling of a pair of symmetrical heated blocks placed inside a rectangular enclosure of aspect ratio two, Int. J. Therm. Environ. Eng. 16 (1) (2018) 1–10.
[60] M. Nazeer, K. Ramesh, H. Farooq, Q. Shahzad, Impact of gold and silver nanoparticles in highly viscous flows with different body forces, Int. J. Model. Simul. 43 (4) (2023) 376–392.
[61] Y.J. Xu, M. Nazeer, F. Hussain, M.I. Khan, M.K. Hameed, N.A. Shah, J.D. Chung, Electroosmotic flow of biological fluid in divergent channel: drug therapy in compressed capillaries, Sci. Rep. 11 (1) (2021) 23652.
[62] M. Nazeer, W. Ali, F. Hussain, Tracking multiphase flows through steep reservoirs with external constraint, Water 15 (18) (2023) 3300.
[63] M. Nazeer, M.W. Nazir, N. Ali, T. Javed, S.A. Abdelmohsen, M.I. Khan, Momentum and thermal transport analysis in MHD nanofluid through the thermally heated square conduit: Finite element method, J. Magn. Magn. Mater. 580 (2023), 170954.
[64] M. Nazeer, M.Z. Alqarni, F. Hussain, S. Saleem, Computational analysis of multiphase flow of non-Newtonian fluid through inclined channel: heat transfer analysis with perturbation method, Comput. Part. Mech. (2023) 1–11.